Nonlinear Processing and Analysis of Angular Signals

Nikos Nikolaidis, *Member, IEEE* and Ioannis Pitas, *Senior Member, IEEE*

***Abstract*— Physical quantities referring to angles, like vector direction, color hue, etc., exhibit an inherently periodic nature. Due to this periodicity, digital filters and edge operators proposed for data on the line cannot be applied on such data. In this paper, we introduce filters for angular signals (circular mean, circular median, circular α-trimmed mean, circular modified trimmed mean). Particular emphasis is given to the circular median filter, for which some interesting properties are derived. We also use estimators of circular dispersion to introduce edge detectors for angular signals. Three variations for the extension of quasirange to circular data are proposed, and expressions for their output pdf are derived. These "circular" quasiranges have good and user-controlled properties as edge detectors in noisy angular signals. The performance of the proposed edge operators is evaluated on angular edges, using certain quantitative criteria. Finally, a series of experiments featuring one-dimensional (1-D) angular signals and hue images is used to illustrate the operation of the new filters and edge detectors.**

I. Introduction

THE GREAT majority of signal processing literature deals with signals whose domain is a straight line. However, certain applications exist where the need to process angular data arises. Such an application comes from color image processing. In HSI, HSV, HLS, $L^*C^*_{ab}h^*_{ab}$, and $L^*C^*_{uv}h^*_{uv}$ color representation systems that are used in computer graphics [1] and color image analysis, hue is essentially a measure of direction. Instantaneous frequency (IF) estimates, which are of particular importance for applications like radar signal processing, seismic signal processing, and underwater acoustics, are angular in nature and should be processed (e.g., smoothed) as such [2]. Another area where angular signals can occur is multichannel signal processing; representation of vectors by means of vector direction angle and vector magnitude, i.e., in a polar coordinate system, can provide a natural context to deal with certain problems. Applications that involve vector direction manipulation (estimation of wind direction from noisy wind velocity data or vehicle direction estimation) can be good candidates for treatment in polar coordinates. Phase information is also angular and should be treated accordingly.

Physical quantities referring to angles are called *angular*, *directional*, or *circular* data. Two-dimensional (2-D) angular signals will be called angular images. Angular data exhibit an inherently periodic nature. Due to this periodicity, the statistical theory used for data on the line cannot be used to deal with such quantities. This is probably the main obstacle to the extended use of angular data processing/analysis in digital signal and image processing. For example, very useful color domains, e.g., HSI, HSV, HLS, that match best the actual human perception of color, were left solely to computer graphics people because the image processing specialists did not like the periodicity of hue and the discontinuity of its domain.

Fortunately, a special statistical theory, called the theory of angular or directional statistics, has been developed to deal with angular data. A complete and comprehensive review of angular statistics can be found in [5]. An extensive list of references on directional statistics can be found in [6]. In this paper, we use the theory of angular statistics and, particularly, the part related to location estimation, to introduce a number of filters (circular mean and median filter) for angular signals. Special attention is paid to circular median filter for which the output pdf and some novel interesting properties (the edge preservation and impulse rejection property) are derived. The pdf for which the circular median filter is the ML estimator of location is also derived. A novel notion of ordering for angular data is proposed. Based on this ordering principle, we extend some order statistics filters (α-trimmed mean, modified trimmed mean filter) to handle angular data. The properties of the new class of circular filters are illustrated by experiments involving 1-D angular signals. Furthermore, the proposed filters are successfully applied in color hue estimation from noisy color images. Another class of multichannel filters that operate in the direction-magnitude domain (the so-called vector directional filters) have been proposed recently [3]. These filters separate the processing of vector data to directional processing and magnitude processing. Fuzzy versions of the same filters have also been proposed [4]. Vector directional filters were applied successfully in noisy color image filtering.

Analysis of angular signals (segmentation, edge detection, feature extraction, etc.) can be also of interest in many applications. Hue image edge detection and segmentation are particularly important since they provide luminance invariant segmentation/edge detection. Such an invariance is crucial for many color image processing applications (e.g., traffic sign recognition or recognition of color-coded objects in industrial applications) since luminance changes (e.g., shadows) render image analysis more difficult. The circular filters proposed in this paper can be used as a preprocessing stage in such a hue-based segmentation. Hue and saturation were used in [8] to

Manuscript received May 10, 1995; revised September 12, 1997. The associate editor coordinating the review of this paper and approving it for publication was Prof. Gonzalo Arce.

N. Nikolaidis is with the Artificial Intelligence and Information Processing Laboratory, Department of Informatics, University of Thessaloniki, Thessaloniki, Greece.

I. Pitas is with the Department of Informatics, University of Thessaloniki, Thessaloniki, Greece.

Publisher Item Identifier S 1053-587X(98)08702-9.

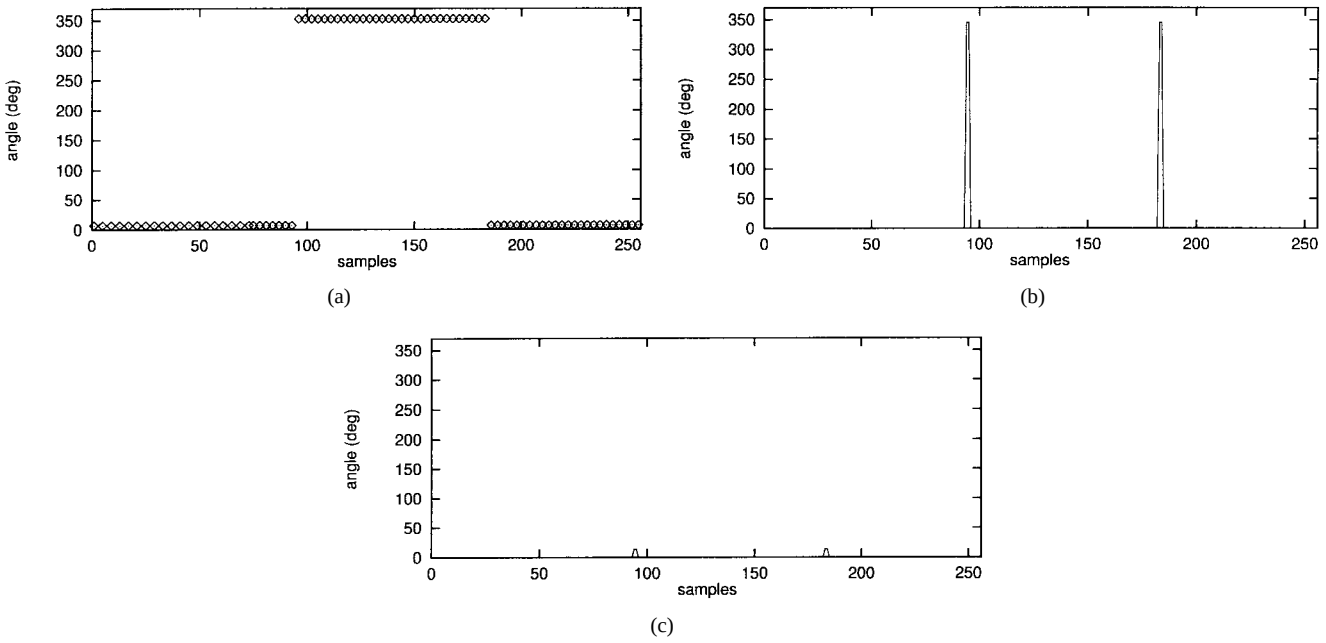

Fig. 1. (a) Original angular signal. (b) Output of a grayscale range edge detector. (c) Output of a circular range edge detector.

segment human faces from the background. In [7], hue alone is successfully used for color image segmentation. Segmentation of color images based on the direction (i.e., the chromaticity) of the RGB vectors is proposed in [9]. In [10], the angular dispersion of the intensity gradient direction is used as an indicator for the existence of an edge.

In this paper, we will concentrate on edge detection on angular signals. Detection of edges on angular signals cannot be done using standard edge detectors. To give an example, a standard range edge detector applied on the one-dimensional (1-D) angular signal shown in Fig. 1(a) detects an edge of height 340° [Fig. 1(b)] between the two homogeneous regions with values 10° and 350°, respectively, whereas the circular range edge detector [Fig. 1(c)] that will be described in Section III estimates the real edge height, i.e., 20° (the smallest arc joining the points related to angles 10°, 350° on the unit circle). Therefore, new edge detectors have to be introduced for data of periodic nature. In this paper, we use measures of angular dispersion that have been proposed in the statistical literature (sample circular variance, circular mean difference, circular range) to introduce edge operators for angular data. We also proceed further by introducing three new noise-robust extensions (the circular quasirange the modified circular quasirange and the median-based circular quasirange) of the notion of quasirange for angular data. Expressions for the output pdf of the circular quasirange and the modified circular quasirange are derived.

This paper is organized as follows. Section II contains some basic notions and definitions from the theory of angular statistics. Novel filter structures for the filtering of angular data are introduced, and some interesting properties are derived. In Section III, we give definitions for angular measures of dispersion that can be used as edge detectors. Three extensions of the quasirange for angular data are proposed. In Section IV, simulations involving one-dimensional (1-D) signals are used to exemplify the operation of the proposed filters, whereas experiments on hue images help compare their performance in hue estimation with other filters acting on the RGB domain. Experimental performance evaluation of the proposed edge detectors along with edge detection experiments on noisy hue images are also presented in the same section. Conclusions follow.

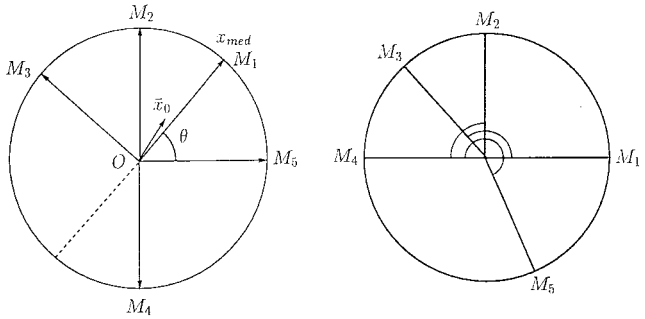

Fig. 2. (a) Sample mean direction $\overline{x_0}$ and the sample median direction x_{med}. (b) Circular range (arc M_5M_4), the CQR of order $i = 1$ (arc M_1M_3), and the MCQR of order $i = 1$ (arc M_2M_4) for $N = 5$ angular data points.

II. Processing of Angular Signals

A. Location Measures for Directional Data

Directional data can be represented as points on a unit circle. An angular observation θ is represented by a point M_1 on a unit circle centered at point O such that the angle between OM_1 and the horizontal axis OX, which is measured in the counterclockwise direction, equals θ. The same observation can also be represented as a unit vector $\mathbf{OM_1}$ [Fig. 2(a)]. Because of the periodicity of angular data, the pdf of a directional random variable is also periodic with a period of 2π. Measures of location for angular data should take under consideration their periodic nature. The classical measures of

location, which are proposed for use with data on a line, depend on the choice of the zero direction on the circle. Therefore, new measures of location that will be invariant to the change of origin must be defined. The *mean direction* μ_0 [5] of an angular random variable θ is defined as the phase angle of the resultant vector $\alpha + j\beta = \rho e^{j\mu_0}$, where

$$\alpha = E[\cos\theta], \quad \beta = E[\sin\theta], \quad \rho = E[\cos(\theta - \mu_0)]. \quad (1)$$

The *sample mean direction* $\overline{x_0}$ of N observations $\theta_1, \ldots, \theta_N$ represented by sample points $M_1, \ldots, M_N$ on a unit circle centered at point O is the direction of the mean resultant vector $\mathbf{R}$ of the unit vectors $\mathbf{OM_1} \cdots \mathbf{OM_N}$ [Fig. 2(a)]. Its value is given by

$$\overline{x_0} = \arctan\left(\frac{\bar{S}}{\bar{C}}\right), \quad \bar{C} = \frac{1}{N}\sum_{i=1}^{N}\cos\theta_i, \quad \bar{S} = \frac{1}{N}\sum_{i=1}^{N}\sin\theta_i. \quad (2)$$

The sample mean direction is proven to be the maximum likelihood estimator of location for data distributed according to the von Mises distribution [5]

$$g(\theta; \mu_0, k) = \frac{1}{2\pi I_0(k)}\exp(k\cos(\theta - \mu_0)) \quad 0 \le \theta < 2\pi, \quad k > 0, \quad 0 \le \mu_0 < 2\pi \quad (3)$$

where $I_0(k)$ is the modified Bessel function of the first kind and order zero. The parameter μ_0 is the mean direction, whereas the parameter k is the concentration parameter of the distribution.

The *median direction* ξ_0 [5] of an angular random variable distributed according to pdf f is the solution of the equation

$$\int_{\xi_0}^{\xi_0+\pi} f(\theta)\,d\theta = \int_{\xi_0+\pi}^{\xi_0+2\pi} f(\theta)\,d\theta = 1/2 \quad (4)$$

with the additional constraint that $f(\xi_0) > f(\xi_0 + \pi)$. The *sample median direction* x_{med} of a set of sample points around the unit circle is the point that divides, by the diameter that passes through it, the rest of the points in two equal subsets [Fig. 2(a)]. The previous definition holds for an odd number of samples. The sample median direction for a set of angular observations is different from the "classical" median [11] of these points. In the following, the term *standard median* will be used for this median to distinguish it from the sample median direction. The sample median direction is not always unique. This can be an inconvenient property if we want to use sample median direction, in practice, for angular signal filtering. Luckily enough, the following property [5] can be used to resolve this ambiguity.

Let $\theta_1 \cdots \theta_N$ be a set of points and a a direction on the unit circle. Then, the sample median direction minimizes the following measure of dispersion around a:

$$d_0 = \frac{1}{N}\sum_{i=1}^{N}\text{arc}(\theta_i, a) \quad (5)$$

$$\text{arc}(\theta_i, a) = \pi - |\pi - |\theta_i - a|| \quad (6)$$

where $\text{arc}(\theta_i, a)$ is the smallest of the two angles that are defined by the points a and θ_i on the unit circle. d_0 is called *circular mean deviation*. In the case of multiple sample median directions, one of them will result in the global minimum for (5), whereas the rest will be local minima. Therefore, d_0 can be used to define a median for circular data that will be unique and, thus, useful in practice. The term arc distance median (ADM) has been introduced in [12] to define the observation that minimizes d_0, and we have adopted the same terminology. The output vector of basic vector directional filter (BVDF) proposed in [3] is the vector whose direction is the ADM of the directions of the input vectors.

B. Circular Filters: Definitions and Some Properties

The direction estimators that have been presented in the previous section can be used to introduce filters for angular signals. These filters will be called *circular filters* in contrast with the filters for data on the line that will be referred to as *standard filters*. One-dimensional *circular mean* and *circular median* filters of size $N = 2\nu + 1$ can be defined by the input–output relations

$$y_i = \text{sample mean direction}(x_{i-\nu}, \ldots, x_i, \ldots, x_{i+\nu}) \quad (7)$$

$$y_i = \text{ADM}(x_{i-\nu}, \ldots, x_i, \ldots, x_{i+\nu}) \quad (8)$$

where y_i is the output value, and $x_{i-\nu}, \ldots, x_i, \ldots, x_{i+\nu}$ are the input samples. Expressions for the 2-D counterparts of the previously defined filters can be easily deduced.

We have proven that the output pdf f_{ADM} of the 1-D circular median filter of length N is given by

$$f_{\text{ADM}}(x) = Nf(x)\int_0^{2\pi}\int_0^{2\pi}\cdots\int_0^{2\pi} f(w_1)\cdots f(w_{N-1}) \times \mathbf{I}(A)\,dw_1\cdots dw_{N-1}, \quad 0 \le x < 2\pi \quad (9)$$

where $\mathbf{I}(A)$ is the indicator function that equals unity when the event A holds and zero otherwise. In our case, A is the event

$$\pi - \frac{1}{N}\sum_{i=1}^{N-1}|\pi - |w_i - x|| < \pi - \frac{1}{N}\left(\sum_{i=1}^{N-1}|\pi - |w_i - w_k|| + |\pi - |x - w_k||\right) \quad \forall k, \quad k = 1\cdots N-1 \quad (10)$$

which makes x the ADM of the N points $x, w_1, \ldots, w_{N-1}$. The proof is given in Appendix A. The theoretical output pdf of a circular median filter applied on data distributed according to von Mises distribution $k = 4$ for filter lengths $N = 3$, $N = 5$ can be seen in Fig. 3.

We have shown that ADM is the maximum likelihood estimator of location for the distribution with the pdf

$$f(\theta) = \frac{1}{2(1 - e^{-\pi})}e^{|\pi - |\theta|| - \pi}, \quad 0 \le \theta < 2\pi. \quad (11)$$

The proof is given in Appendix B.

It can be easily proven that if at least $\nu + 1$ out of the $N = 2\nu + 1$ points inside the 1-D circular median window have the same value x, then the output of the filter is x, which is a property that also holds for the standard median. Therefore, in the case of bilevel angular signals, the output of the standard

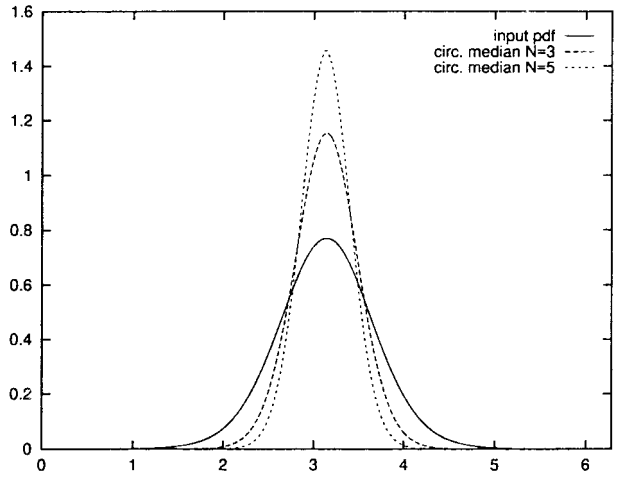

Fig. 3. Output pdf of circular median filters of length $N = 3$ and $N = 5$ for input data distributed according to $k = 4$, $\mu_0 = \pi$ von Mises distribution.

median and the circular median are identical and equal to the most frequent sample. As a result, a number of properties that hold for the standard median on bilevel signals [13] also apply to the circular median filter. The circular median filter has edge preservation properties similar to those of the standard median. It does not corrupt an edge modeled as step function. In contrast, the circular mean smooths a step edge to a ramp function. Furthermore, the circular median filter effectively removes impulses in contrast with the circular mean filter, which fails completely in this type of noise. The probability of correct signal reconstruction for the circular median filter of length N, in constant signal areas corrupted with impulsive noise having probability of occurrence p, equals the probability that less than half of the observations inside the median window are corrupted by the noise

$$P(\text{correct reconstruction}) = \sum_{k=0}^{\frac{N-1}{2}} \binom{N}{k} p^k (1-p)^{N-k}. \quad (12)$$

In order to define general order statistics filters for angular data, we must introduce the notion of angular data ordering. The new ordering scheme should take under consideration the periodic nature of the data. This requirement inhibits the use of standard Cartesian ordering. Furthermore, the new scheme should be coherent with the definition of sample median direction. An ordering scheme that meets the above needs is the following.

Let us denote by $\theta_{[k]}$ the kth ordered sample on the circle. Let $\theta_1, \theta_2, \ldots, \theta_N$ be samples distributed according to some circular distribution, and let $\theta_{(1)}, \theta_{(2)}, \ldots, \theta_{(N)}$ be the Cartesian ordered samples, i.e.,

$$\theta_{(1)} \le \theta_{(2)} \le \cdots \le \theta_{(N)}. \quad (13)$$

We calculate first the arc distance median $\theta_{\text{med}} \triangleq \theta_{[\frac{N+1}{2}]}$. Let us suppose that θ_{med} corresponds to $\theta_{(i)}$. The rest of the ordered samples can be defined by

$$\theta_{[k+\frac{N+1}{2}]} = \theta_{(\text{mod}_N(i+k))}, \quad -\frac{N-1}{2} \le k \le \frac{N-1}{2} \quad (14)$$

where $\text{mod}_N(\cdot)$ denotes the modulo N operator. This ordering scheme can be used to detect, and subsequently remove, extreme observations. However, due to the periodicity of the angular data, no minimum or maximum observation can be specified. The proposed scheme can be better described as ordering in terms of centrality, the median being at the central most position and the rest of the samples being ordered in pairs of descending centrality

$$\theta_{[\frac{N+1}{2}]}, \left(\theta_{[\frac{N+1}{2}-1]}, \theta_{[\frac{N+1}{2}+1]}\right), \left(\theta_{[\frac{N+1}{2}-2]}, \theta_{[\frac{N+1}{2}+2]}\right), \ldots \left(\theta_{[1]}, \theta_{[N]}\right). \quad (15)$$

Other ordering principles for angular data (angular Tukey's depth, angular simplicial depth, arc distance depth) have also been proposed in the statistical literature. Some of them are summarized in [14]. A more detailed description of these principles along with a discussion on their advantages and disadvantages can be found in [12]. It is worthwhile to observe that the notion of outliers is somewhat different for circular data because angular distributions have bounded support. On the line, the more extreme the value x of an outlier, the greater the distance from the main data mass. However, in the case of circular data, there is limited space for an observation to outlie. Consider, for example, the following observations: 5 20 33 40 50 351. If these observations represent data on the line, then the point 351 can be safely recognized as outlying. However, if these numbers represent angular data (in degrees), then 351 is in perfect agreement with the rest of the data. Due to the bounded support of angular data, outliers can be easily detected only when the observations are sufficiently concentrated around a particular point. The angular deviation (6) between a data point and the population sample mean or median direction can be used to tell whether the observation is outlying or not. Four statistical tests for outliers among angular data can be found in [15]. With certain modifications, some of these statistics can be utilized in angular data ranking.

Having defined the way that the circular data are ordered, the derivation of the various-order statistics filters is straightforward. For example, the 1-D *circular α-trimmed mean filter* [11] of length $N = 2\nu + 1$ has the definition

$$y_a = \text{sample mean direction}\left(x_{[\alpha N+1]}, \ldots, x_{[\frac{N+1}{2}]}, \ldots x_{[N-\alpha N]}\right) \quad 0 \le \alpha < 0.5 \quad (16)$$

where $\alpha N + 1$, $N - \alpha N$ are considered to be integers, and $x_{[k]}$ are the ordered input samples $x_{i-\nu}, \ldots, x_{i+\nu}$. Parameter α controls the number of the smaller and the bigger samples in the filter window that will be rejected as outliers. Another order-statistics-based filter that can be easily modified to handle angular data is the modified trimmed mean filter [11]. The 1-D *circular modified trimmed mean* (CMTM) of length $N = 2\nu + 1$ can be defined as

$$y_i = \text{sample mean direction}(x_{i+k} \mid \text{arc}(x_{i+k}, x_{\text{med}}) < q \quad -\nu \le k \le \nu) \quad (17)$$

where x_{med} is the ADM of samples $x_{i-\nu}, \ldots, x_{i+\nu}$. The circular modified trimmed mean filter excludes samples that differ considerably from the local circular median. The number of rejected samples is controlled by the parameter q.

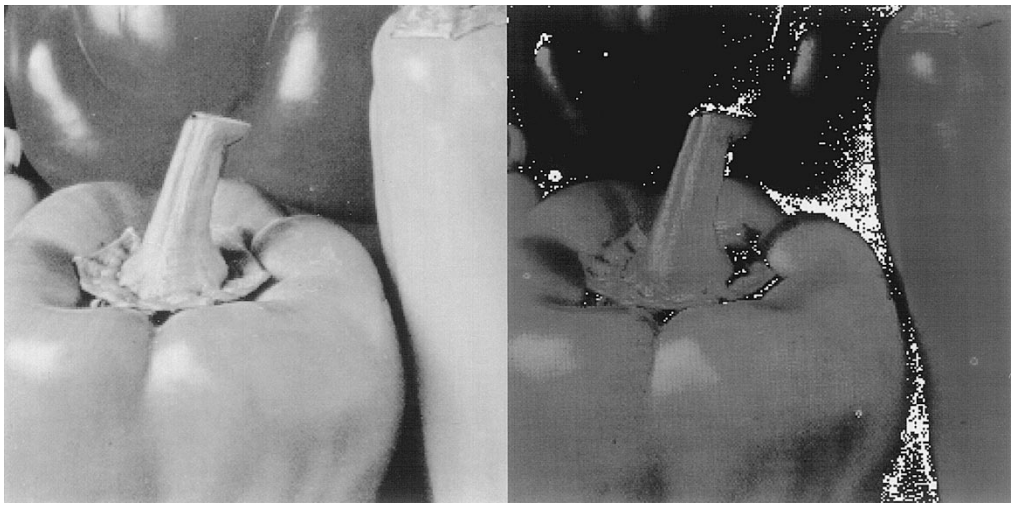

(a) (b)

Fig. 4. (a) "Pepper" test color image, size 256×256. (b) Hue color component of test image "Pepper."

III. Angular Signal Edge Detection

A. Measures of Angular Dispersion

Circular measures of dispersion can be used as edge detectors for angular data since edges are areas having large local signal variance. The *circular variance* [5] of an angular random variable θ is such a measure. It is defined as

$$V_0 = 1 - E[\cos(\theta - \mu_0)] \tag{18}$$

where μ_0 is the mean direction of θ. The *sample circular variance* S_0 of N angular data points $X_1, \ldots, X_N$, $0 \le X_i < 2\pi$ takes values in the interval $[0, 1]$ and is defined as

$$S_0 = 1 - \frac{1}{N} \sum_{i=1}^{N} \cos(X_i - \bar{X}_0) \tag{19}$$

where $\bar{X}_0$ is the sample mean direction (2). The *circular mean difference* $\bar{D}_0$ [5] is another useful measure of dispersion. It is defined by

$$\begin{aligned} \bar{D}_0 &= \frac{1}{N^2} \sum_{i=1}^{N} \sum_{j=1}^{N} \text{arc}(X_i, X_j) \\ &= \frac{1}{N^2} \sum_{i=1}^{N} \sum_{j=1}^{N} \{\pi - |\pi - |X_i - X_j||\} \end{aligned} \tag{20}$$

where $\text{arc}(X_i, X_j)$ is the deviation (6) between two angles X_i and X_j. The *circular range* is defined as the length of the smallest arc that includes all the sample observations [Fig. 2(b)]. The circular range can be evaluated as

$$w = 2\pi - \max(T_1, \ldots, T_N) \tag{21}$$

where T_k are measures of the arcs between adjacent samples

$$\begin{aligned} T_k &= X_{(k+1)} - X_{(k)}, \quad k = 1, \ldots, N-1 \\ T_N &= 2\pi - X_{(N)} + X_{(1)} \end{aligned} \tag{22}$$

and $X_{(1)}, X_{(2)}, \ldots, X_{(N)}$ are the Cartesian ordered directional samples $X_1, X_2, \ldots, X_N$.

All the above measures of dispersion can be used to detect angular edges. For example, a 2-D edge detector for angular images that is based on the circular mean difference can be defined by the input–output relation

$$y_{ij} = \text{circular mean difference}(X_{i+r,j+s}; (r,s) \in A) \tag{23}$$

where A is the edge detector window, $X_{i+r,j+s}$ are the input samples inside this window, and y_{ij} is the detector output.

B. Circular Quasirange

Unfortunately, the edge detectors described in Section III-A have poor performance when acting on noisy angular signals. This is illustrated in Fig. 5, where the output of a 5×5 circular mean difference edge detector operating on the hue component of image "Pepper" (Fig. 4) corrupted by impulsive noise acting independently on each RGB channel can be seen. In the following, we shall introduce extensions of the circular range, i.e., circular quasiranges, that are suitable for edge detection on noisy angular signals. Their big advantage is that they allow noise suppression to be done along with edge detection, thus making the edge detector operator more robust. Noise suppression is achieved by leaving out a certain amount of extreme points (that depends on the order of the quasirange).

In the case of data on the line, the ith quasirange of N observations is defined by

$$x_{(i)} = x_{(N-i)} - x_{(i+1)}. \tag{24}$$

The first way to extend this definition to circular data is by making use of the circular range (21). The circular quasirange w_i of order i, $(0 \le i < (N-1)/2)$ for N angular observations (N odd) can be found by evaluating the circular range w and "stripping" out i data points from each of the two ends of the arc w. The arc that includes all data points except for the $2 \cdot i$ points that have been rejected [Fig. 2(b)] will be called the ith-order *circular quasirange* (CQR). For $i = 0$, CQR and circular range (21) are equivalent.

The evaluation of the output pdf for the circular quasirange, when this is applied on a noisy angular edge modeled as

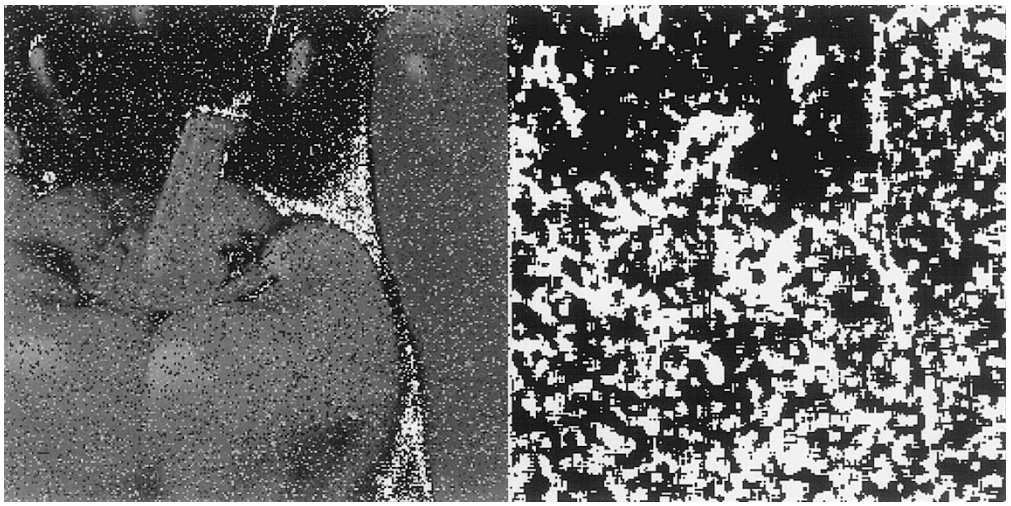

(a) (b)

Fig. 5. (a) Hue component of test image "Pepper" corrupted by 10% impulsive noise of impulse value 255 acting independently on each RGB channel. (b) Output of a 5×5 circular mean difference edge detector (threshold $T = 28$).

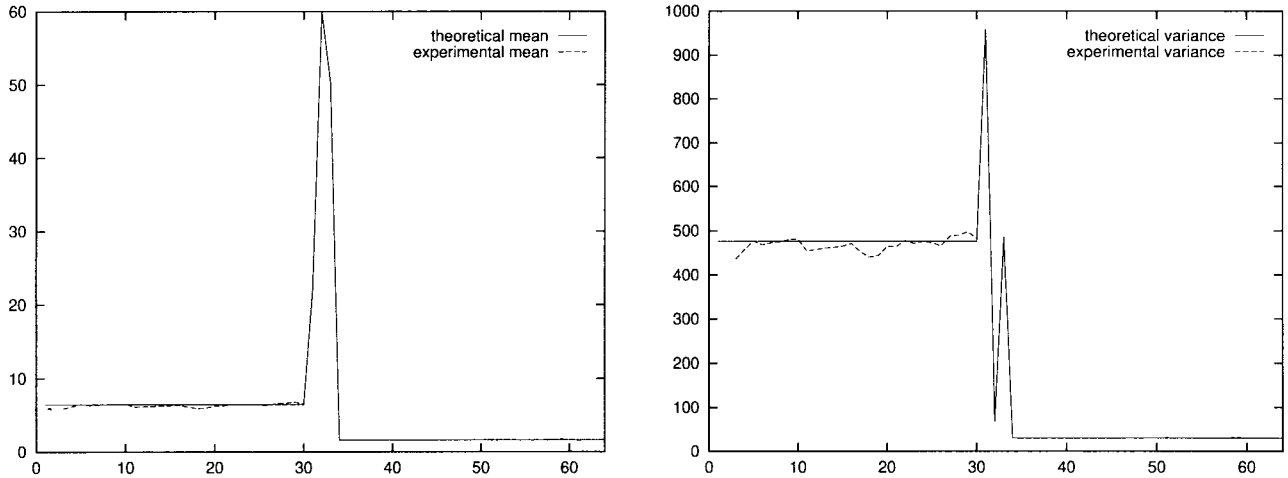

(a) (b)

Fig. 6. Theoretical (solid line) and experimental (dashed line) (a) mean and (b) variance of the response of a circular quasirange edge detector of order $i = 1$ and $N = 5$ on a step edge corrupted by impulsive noise of constant impulse value.

a step function, is very cumbersome for a general noise distribution. In Appendix C, we present the output pdf of a circular quasirange operator of length N and order i for the tractable case of impulsive noise of constant impulse value m_n and probability of occurrence p that corrupts a 1-D angular edge of the form

$$s(k) = \begin{cases} m_{s1} & 0 \le k \le l \\ m_{s2} & l < k \le M \end{cases} \tag{25}$$

Fig. 6 depicts the theoretical and experimental mean and variance for a circular quasirange of order $i = 1$ and window length $N = 5$ applied on an edge-bearing signal (25) having $M = 64$, $l = 32$, $m_{s1} = 40$, and $m_{s2} = 100$. The edge is corrupted by impulsive noise of impulse value $m_n = 120$ and probability of occurrence $p = 0.1$. It can be seen that theoretical and simulation results are in perfect agreement. The large mean output value of the circular quasirange response on the edge, compared with the small mean output value in the homogeneous regions, clearly indicates that CQR can be used as an edge detector. Note that the mean output value at the edge is 60, i.e., the actual edge height.

A second way of defining the circular quasirange is through the utilization of the angular data ordering that is based on the arc distance median. Let $X_{[1]}, \ldots, X_{[N]}$ be N angular samples ordered according to this ordering principle. Then, the ith-order *median-based circular quasirange* (MBCQR) is given by

$$w_i' = \text{arc}_{\text{med}}\left(X_{[1+i]}, X_{[N-i]}\right)$$

where arc_{med} denotes the arc on the unit circle that is limited by points $X_{[1+i]}$, $X_{[N-i]}$, and includes the arc distance median. It is obvious that in general, $w_i \neq w_i'$. However, simulations with noisy images showed that edge detectors based on CQR and MBCQR produce almost the same output.

A third definition for the circular quasirange of N data points can be the following: We define as *modified circular*

quasirange (MCQR) W_i of order i the smallest arc that contains all points except for $2 \cdot i$ successive points [Fig. 2(b)]. For $i = 0$, MCQR coincides with the circular range (21). Modified circular quasirange W_i can be evaluated in the following way: We order in the Cartesian way the directional samples $X_1, X_2, \ldots, X_N$ and evaluate arc lengths T_k between points being $\Delta = 2i + 1$ samples apart in a circular manner, i.e.,

$$T_k = \begin{cases} X_{(\Delta+k)} - X_{(k)} & 1 \le k \le N - \Delta \\ 2\pi + X_{(\mathrm{mod}_N(\Delta+k))} - X_{(k)} & N - \Delta < k \le N \end{cases} \tag{26}$$

where $\mathrm{mod}_N(\cdot)$ denotes the modulo N operator. W_i is then given by

$$W_i = 2\pi - T_{\max} = 2\pi - \max(T_1, \ldots, T_N). \tag{27}$$

Since MCQR W_i is evaluated using Cartesian ordering of data samples, the output pdf of the related edge detector in constant signal regions corrupted by additive noise can be evaluated using the theory of order statistics on the line. We have proven that the output pdf f_{W_0} of the 1-D MCQR W_i for $i = 0$ (i.e., the circular range) for constant signal areas corrupted by zero-mean additive noise having pdf $f(\theta)$ is given by

$$f_{W_0}(x) = f_{T_{\max}}(2\pi - x) \tag{28}$$

$$\begin{aligned} f_{T_{\max}}(x) = N! \cdot \Bigg(& \int_0^x \cdots \int_0^x \Bigg\{ \int_0^{2\pi} f(v - v_{N-1} \\ & - \cdots - v_2 - x) f(v - v_{N-1} - \cdots - v_2) \\ & \cdots f(v - v_{N-1}) f(v)\, dv \Bigg\} \cdot u(2\pi - x \\ & - v_2 - \cdots - v_{N-1}) \cdot u(2x - 2\pi + v_2 \\ & + \cdots + v_{N-1})\, dv_2 \cdots dv_{N-1} + \int_0^x \cdots \int_0^x \\ & \Bigg\{ \int_0^{2\pi} f(v - v_{N-1} - \cdots - x - v_1) f(v \\ & - v_{N-1} - \cdots - x) \cdots f(v - v_{N-1}) f(v)\, dv \Bigg\} \\ & \cdot u(2\pi - v_1 - x - v_3 - \cdots - v_{N-1}) \\ & \cdot u(2x - 2\pi + v_1 + v_3 + \cdots + v_{N-1})\, dv_1\, dv_3 \\ & \cdots dv_{N-1} + \cdots + \int_0^x \cdots \int_0^x \Bigg\{ \int_0^{2\pi} f(v - x \\ & - v_{N-2} - \cdots - v_1) f(v - x - v_{N-2} - \cdots - v_2) \\ & \cdots f(v - x) f(v)\, dv \Bigg\} \cdot u(2\pi - v_1 - v_2 - \cdots \\ & - v_{N-2} - x) \cdot u(2x - 2\pi + v_1 + \cdots + v_{N-2})\, dv_1 \\ & \cdots dv_{N-2} + \int_0^x \cdots \int_0^x \Bigg\{ \int_0^{2\pi} f(v - 2\pi + x) f(v \\ & - v_{N-1} - \cdots - v_2) \cdots f(v - v_{N-1}) f(v)\, dv \Bigg\} \\ & \cdot u(2\pi - v_2 - \cdots - v_{N-1} - x) \cdot u(2x - 2\pi + v_2 \\ & + \cdots + v_{N-1})\, dv_2 \cdots dv_{N-1} \Bigg). \end{aligned} \tag{29}$$

The proof can be found in Appendix D. The pdf of W_i for $i > 0$ can be derived using exactly the same methodology, but results will be omitted because the resulting formulae are rather lengthy.

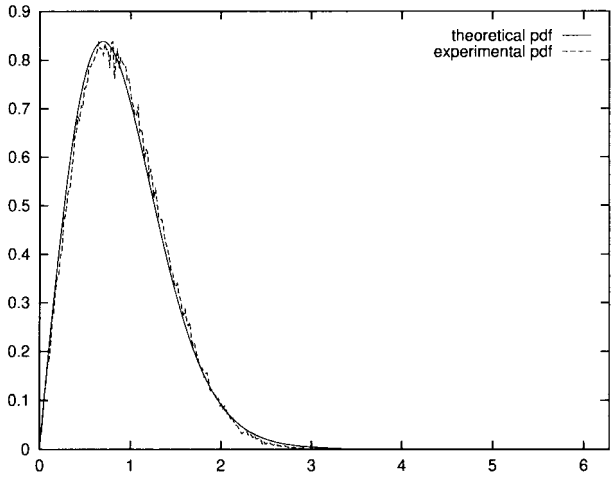

Fig. 7. Theoretical (solid line) and experimental (dashed line) output pdf for the modified circular quasirange of length $N = 3$ and order $i = 0$ for input data distributed according to $k = 4$, $\mu_0 = \pi$ von Mises distribution.

The theoretical output pdf of the circular range for length $N = 3$ when the input data are corrupted by noise distributed according to von Mises distribution can be seen in Fig. 7 along with the experimental pdf. Using the derived pdf, we can evaluate the mean and variance of the edge detector output in constant signal areas and, consequently, choose an appropriate threshold so that the output of the detector at background points does not exceed this threshold. Evaluation of the output pdf for the actual edge region would be of equal importance. However, this is difficult to do since it requires order statistics from dependent, nonidentically distributed random variables.

IV. Experimental Results

A. Circular Filters

In our effort to illustrate the operation of the proposed circular filters and to demonstrate the inability of the standard filters to handle angular data, we have conducted two sets of experiments featuring 1-D angular signals. In the first experiment, a 1-D angular signal (one horizontal line of the hue component of color image "Pepper") [Fig. 8(a)] was corrupted by impulsive noise of constant value 120° and probability of occurrence 20% [Fig. 8(b)]. The output of the standard median filter and the circular median filter applied on the noisy signal can be seen in Figs. 8(c) and (d), respectively. The window size for both filters was $N = 5$. Note that the standard median filter fails to reject the impulses that exist within the segment that includes samples 60 to 120. This failure can be explained by the fact that the samples in this segment have values close to 0° and 360°, which are mistakingly not treated as neighboring ones by the median filter. On the other hand, the circular median filter successfully rejects the impulses in this area by taking into account the periodic nature of the signal. In the second experiment, a 1-D signal (another line from the hue component of "Pepper") [Fig. 9(a)] was corrupted by zero-mean additive von Mises noise having concentration parameter

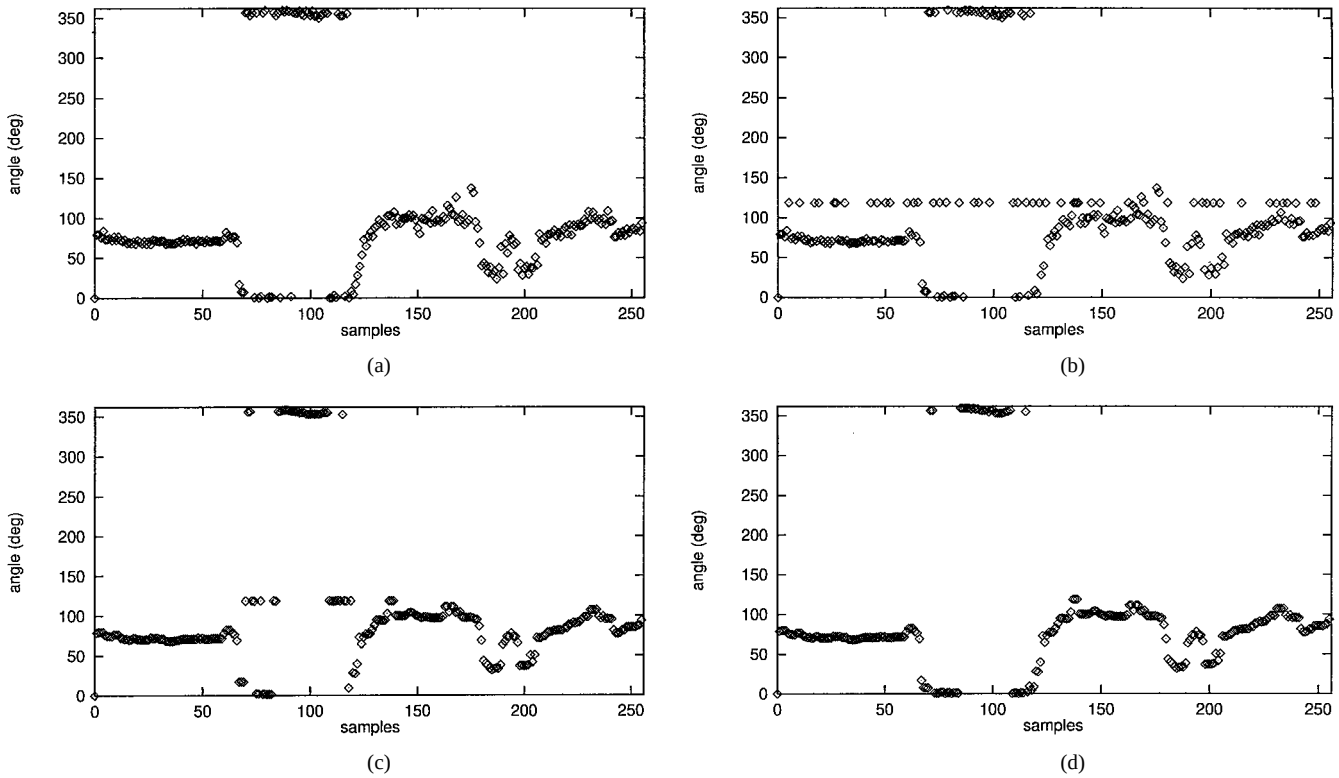

Fig. 8. (a) Original angular signal. (b) Angular signal corrupted by impulsive noise of constant impulse value. (c) Output of a standard median filter having window size $N = 5$. (d) Output of a circular median filter of the same window size.

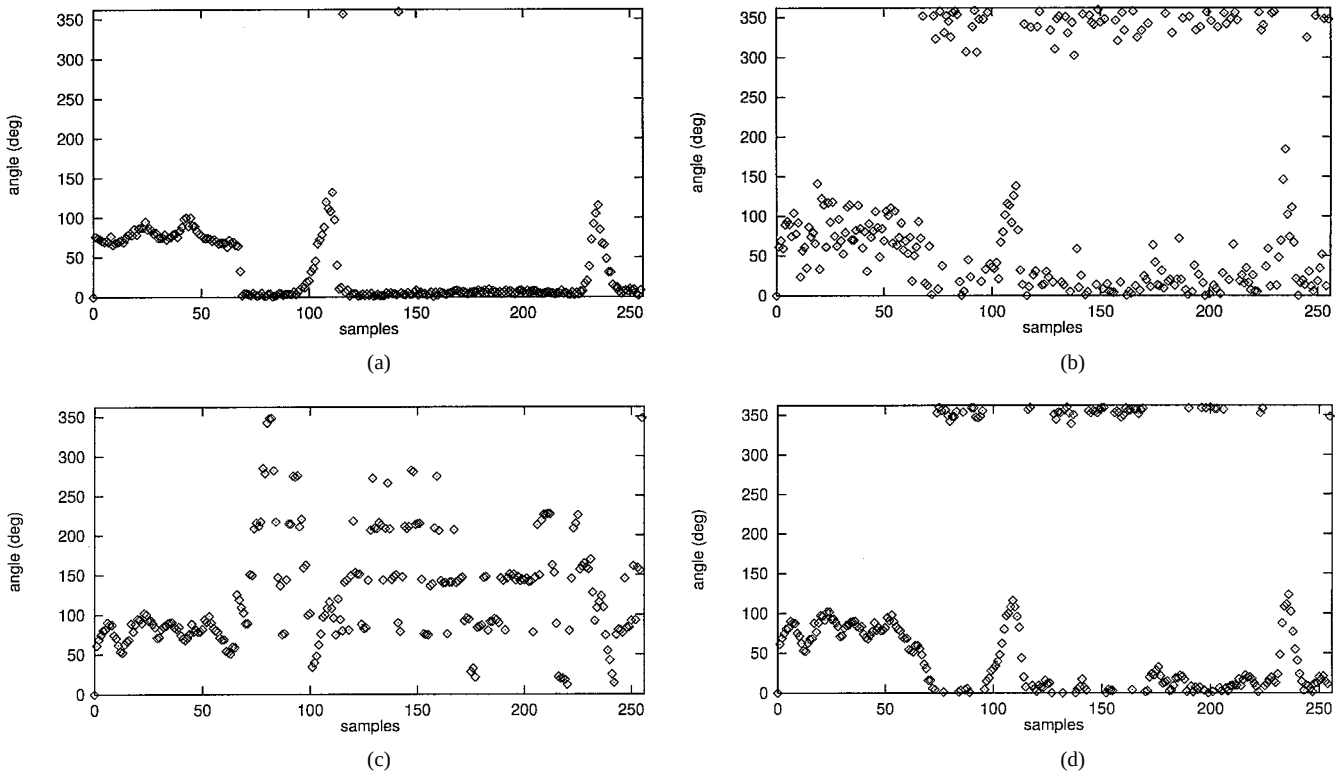

Fig. 9. (a) Original angular signal. (b) Angular signal corrupted by von Mises noise. (c) Output of a standard mean filter having window size $N = 5$. (d) Output of a circular mean filter of the same window size.

$k = 6$. [Fig. 9(b)]. The output of the standard mean filter and the circular mean filter (window size $N = 5$) applied on the noisy signal can be observed in Fig. 9(c) and (d), respectively. It is obvious that the standard mean filter destroys the angular signal, whereas the circular mean filter achieves sufficient noise smoothing. In order not to misinterpret Fig. 9(d), bear in

mind that due to the signal periodicity, samples close to 360° are also very close to 0°.

The effectiveness of the proposed circular filters in the filtering of directional data was further illustrated in two additional sets of experiments dealing with noise filtering in the hue component of color images represented in the HSV color space. HSV is a cylindrical color space that matches best the actual human perception of color [1]. Hue represents the angle around the vertical axis with red being at 0°, green at 120°, and blue at 240°. The test color image "Pepper" of size 256×256 was used for all simulations [Fig. 4(a)]. The hue color component of "Pepper" (called *hue image* from now on), scaled and represented as a gray-level image, can be seen in Fig. 4(b). Due to the the periodic nature of hue, both black and white pixels in this image correspond to red 0°. Intermediate colors are represented as shades of gray. In both experimental settings, we tested the performance of the proposed circular filters in the case of hue estimation on noisy color images. The reason for this investigation is that correct hue estimation is important in many applications (e.g., in graphics, printing arts, or as a preprocessing step for luminance invariant color object segmentation). At this point, we shall make clear that comparing circular filters with RGB domain filters in terms of noise suppression in the RGB domain would be unfair since circular filters operate only on hue, leaving noise imposed on saturation and value intact. However, if full color image filtering is required, the proposed circular filters can be easily integrated with magnitude filters to devise a joint direction/magnitude filtering scheme like the one proposed in [3]. Optimal L filters for the magnitude of vectors corrupted by additive noise have been proposed in [16].

To overcome the fact that standard performance measures cannot be used to evaluate noise suppression in the hue component due to the periodic nature of the angular data, we introduced modifications of the well-known noise reduction index (NRI) and signal-to-noise ratio (SNR). The modifications make them suitable for circular data by substituting standard signal difference with a measure of angular difference, i.e., the deviation (6) between two angular data points. The resulting performance measures will be called *circular noise reduction index* (NRI_c) and *circular signal-to-noise ratio* (SNR_c)

$$\mathrm{NRI}_c = 10 \log \frac{\sum_k (\pi - |\pi - |y(k) - s(k)||)}{\sum_k (\pi - |\pi - |x(k) - s(k)||)}. \quad (30)$$

$$\mathrm{SNR}_c = 10 \log \frac{\sum_k s(k)^2}{\sum_k (\pi - |\pi - |y(k) - s(k)||)^2}. \quad (31)$$

In the previous definitions, $y(k)$, $x(k)$, $s(k)$ are the filtered, noisy, and original angular observations, respectively.

In the third set of experiments, we tested the performance of the proposed angular data filters in the case of hue estimation on color images that were corrupted by various noise models in the RGB color space. Two filter classes were tested and compared: multichannel filters on the RGB domain and circular filters directly on hue. The methodology that was adopted was the following. The original RGB image was first corrupted by one of the following types of multivariate noise:

- additive zero-mean Gaussian noise having standard deviation $\sigma = 20$ on each RGB channel;
- impulsive noise having constant value 255 and probability of occurrence 5% on each channel;
- additive zero-mean Laplacian noise with $\sigma = 14$ on each channel.

Obviously, due to the nonlinear nature of the RGB-HSV transformation, the noise pdf on the hue domain differs from the noise originally imposed on the RGB channels. In the case of multichannel filters operating on Cartesian coordinates, images were filtered in the RGB domain and then transformed to HSV in order to assess filter performance in hue estimation. The following filters were used for comparison:

- marginal (componentwise) median;
- vector median;
- componentwise arithmetic mean.

In the case of circular filters, noisy RGB images were transformed to HSV, the hue component was filtered, and their performance was evaluated. The circular filters that were tested included circular median, circular mean, circular trimmed mean filter ($\alpha = 0.1$ or $\alpha = 0.2$), and circular modified trimmed mean with $q = 30°$ or $q = 100°$. The standard, single-channel mean and median filters were also used to filter hue on the HSV domain. The window size for all filters in this set of experiments was 3×3. The results of the filtering with respect to NRI_c are summarized in Table I. The use of SNR_c instead of NRI_c yields very similar results (the ranking of the various filters remains the same), which will not be reported here due to lack of space. As expected, the standard, single-channel mean, and median filters operating on hue had very bad performance; actually, standard mean destroyed the image. For Gaussian noise, componentwise mean filtering in RGB, which is the MLE for this type of noise in Cartesian coordinates, gave the best hue noise suppression, closely followed by circular mean. The circular trimmed mean filter with trimming coefficient $\alpha = 0.2$ gave the best results in the filtering of Laplacian noise. Finally, in the case of impulsive noise, circular median performed better than vector median.

The fourth set of experiments aimed at investigating the performance of the circular filters in the case of hue estimation in color images where noise was applied directly on hue. Although this scenario might not be realistic in the case of color image data (no sensor produces hue data), we have

TABLE I
CIRCULAR NOISE REDUCTION INDEX NRI_c FOR VARIOUS NOISE MODELS CORRUPTING THE RGB COLOR COORDINATES OR THE HUE COMPONENT OF IMAGE "PEPPER"

	N(0,20)	imp 5%	Lap. $\sigma = 14$	imp1 10%	imp2 10%	M(0,6)
marg. median	-3.18	-3.95	2.87	-1.75	-3.68	-3.25
vector median	-2.06	4.00	2.04	-1.89	-3.76	-2.76
componentwise mean	√ -3.81	-0.29	-2.88	0.77	-1.85	-3.79
standard median	-1.81	-3.10	-1.71	-0.91	-3.04	-0.96
standard mean	3.76	2.99	4.52	3.97	3.62	3.50
circular median	-3.25	√ -4.15	-2.79	√ -2.06	√ -4.06	-3.21
circular mean	-3.61	-1.81	-2.80	0.65	-1.93	√ 3.88
circ. tr. mean 0.1	-3.60	-2.98	-2.92	0.50	-3.05	-3.79
circ. tr. mean 0.2	-3.56	-3.72	√ -2.96	-1.38	-3.69	-3.66
CMTM 30^0	-3.46	-3.69	-2.86	-1.45	-3.66	-3.34
CMTM 100^0	-3.60	-2.10	-2.80	0.21	-2.43	-3.87

included these experiments for two reasons: 1) To give readers an idea of the behavior of the proposed filters in other types of angular signals where such noise models might arise; 2) some noise types cast on the RGB domain might result in hue noise that can be modeled using one of the pdfs discussed bellow. Test image "Pepper" was transformed to HSV, and its hue component was corrupted by the following types of noise:

- impulsive noise of constant value 120° (green) and probability of occurrence 10% (denoted as imp1 in Table I);
- impulsive noise with uniformly distributed impulse value and probability of occurrence 10% (denoted as imp2 in Table I);
- zero-mean additive von Mises noise with concentration parameter $k = 6$.

Filtering was performed using the filters and performance evaluation procedures described in the previous set of experiments. For all filters, the window size was 3×3. The results can be seen in the second part of Table I. As expected, Von Mises noise was filtered more effectively by the circular mean filter, which is the maximum likelihood estimator for this type of noise. On the other hand, the circular median proved to be the best choice for the removal of both kinds of impulsive noise on hue.

Similar results were obtained when we applied the circular filters on the vector direction of noisy vector fields. These results are not presented here due to lack of space.

B. Angular Data Edge Detectors

The quantitative evaluation of edge detector performance, especially in the presence of noise, is not an easy task. Various quantitative criteria have been presented in the literature. In this paper, we have used a quantitative criterion similar to the *edge detection error rate* P_t described in [17] in order to evaluate and compare the performance of the proposed edge detectors for various noise types. Usually, the output of an edge detector is thresholded, and pixels with value over the threshold are considered as edge points. The thresholding operation is therefore crucial for the performance of the edge detector, and the choice of the optimum threshold T_{opt} for a certain type of noise must be done carefully. In the following, we shall define three threshold-dependent quantities that characterize the performance of an edge detector. The probability of false alarm $P_F(T)$ for a given threshold T is the probability of a nonedge point to be classified as an edge, i.e., the probability the output value of the detector at this point to be above the specified threshold. The probability of detection $P_D(T)$ is the probability that an edge point is detected as such. Finally, the probability of nondetection $P_{\text{ND}}(T)$ is the probability an edge point not to be detected as such, i.e., to be classified in the background. An edge detector has good performance if $P_D(T)$ is close to unity (and, therefore, $P_{\text{ND}}(T)$ close to zero) and $P_F(T)$ tends to zero. In order to monitor all three characteristic quantities, we construct the ratio

$$R(T) = \frac{P_F(T) + P_{\text{ND}}(T)}{P_D(T)}. \tag{32}$$

As P_D increases and P_F, P_{ND} tend to zero, $R(T)$ tends to zero. On the other hand, as P_D decreases and P_F tends to unity, $R(T)$ tends to infinity. The smaller the value of $R(T)$, the better the performance of an edge detector. The optimum threshold T_{opt} is the one that minimizes $R(T)$. In the case of an efficient edge detector, the output pdf of the background points will be well separated from the output pdf of the edge points. In this situation, the optimum threshold T totally separates the two groups of points (edge points and background points), achieving a small value for $R(T)$. The performance of different edge detectors on the same type of noise can be assessed by comparing the minimum value $R_{\min} = R(T_{\text{opt}})$. In our experiments, we used $R_{\min}$ to evaluate the performance of CQR and MCQR edge detectors of various orders on synthetic hue edges. Comparisons were limited only to these two detectors because, as it was mentioned earlier, edge operators for data on the line (Sobel, Laplace, Canny, etc.) produce erroneous results when applied on angular data. A 2-D three-channel RGB signal whose cross section contains a step edge on the red and green channels was used in the simulations as

$$\begin{aligned} \text{Red}(k) &= \begin{cases} 80 & 0 \le k < M/2 \\ 50 & M/2 \le k \le M \end{cases} \\ \text{Green}(k) &= \begin{cases} 50 & 0 \le k < M/2 \\ 80 & M/2 \le k \le M \end{cases} \\ \text{Blue}(k) &= 20. \end{aligned} \tag{33}$$

If we transform this signal to HSV, we obtain a hue edge whose cross section is

$$H(k) = \begin{cases} 30^0 & 0 \le k < M/2 \\ 90^0 & M/2 \le k \le M. \end{cases} \tag{34}$$

Two types of noise were used to contaminate independently each of the three channels of the RGB signal: additive Gaussian noise of zero mean and $\sigma = 15$, $\sigma = 25$ and impulsive noise of constant value 255 and probabilities of occurrence $p = 10\%$ and $p = 20\%$. After that, we transformed the noisy signal to the HSV color space and applied the circular quasirange and modified circular quasirange edge detectors of various orders i on the hue signal using a window of size 3×3 or 5×5. Results can be seen in Fig. 10, where $R_{\min}$ is drawn as a function of order i. The performance of the detectors increases ($R_{\min}$ decreases) with i until a maximum is reached and then decreases. This decrease in the detector performance is due to the fact that large values of order i destroy the edge. The order for which the best performance is achieved depends on the noise power. The bigger the power of the noise, the greater the order must be for the edge detector to be able to reject the noisy points. In addition, for the same type of noise, MCQR achieves its minimum $R_{\min}$ value for smaller order i. Diagrams also show that the 5×5 edge detectors have better performance than the 3×3 counterparts and that the performance decreases with the noise power. Comparing MCQR and CQR edge detectors, we can say that the two detectors have almost the same performance for hue edges that correspond to RGB edges corrupted by Gaussian noise. MCQR is better in the case of hue edges resulting from RGB edges corrupted by impulsive noise, especially for $p = 20\%$.

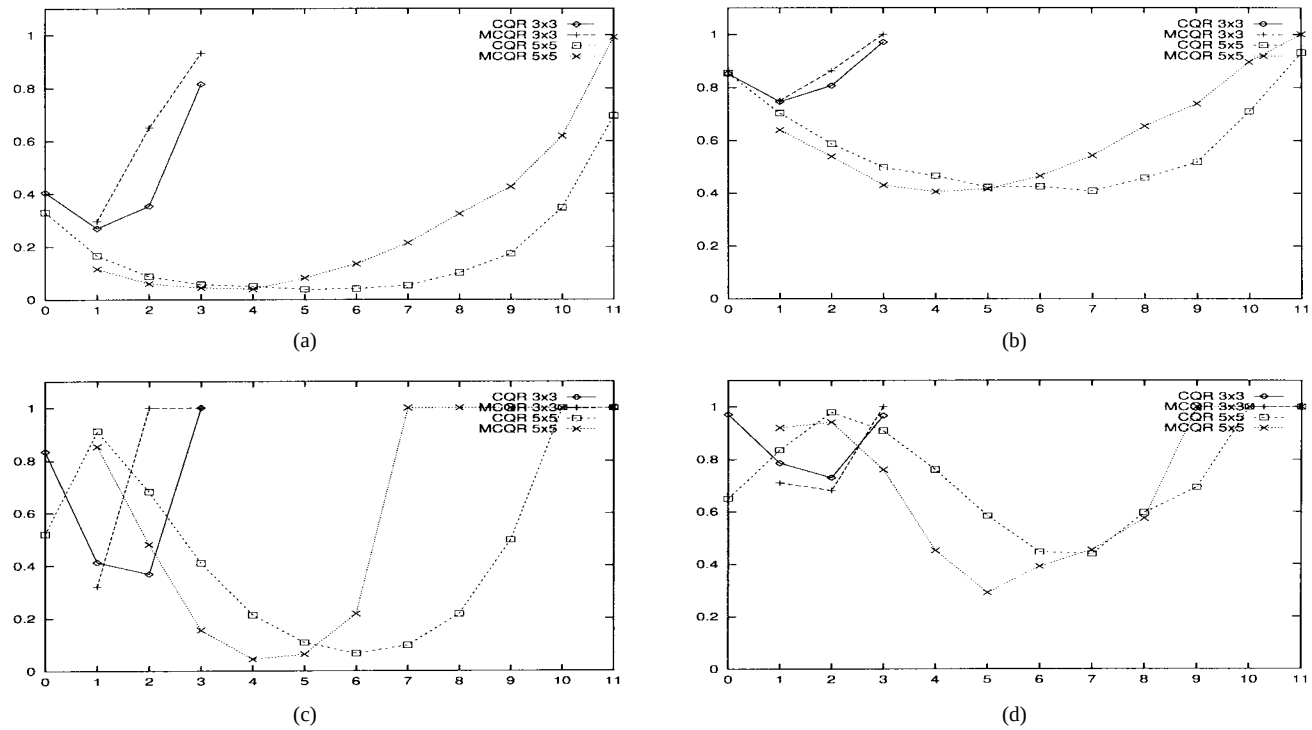

Fig. 10. Figure of merit $R_{\min}$ for CQR and MCQR angular edge detectors of window size 3×3 and 5×5applied on a noisy hue edge, for various orders i. The hue edge resulted from the HSV transformation of an RGB edge corrupted by the following noise types: Gaussian noise of standard deviation (a) $\sigma = 15$ and (b) $\sigma = 25$, impulsive noise of constant value 255 and probability of occurrence (c) $p = 10\%$ and (d) $p = 20\%$ on each RGB channel.

Fig. 11. (a) Output of 5×5 CQR edge detector of order $i = 4$ applied on the hue component [Fig. 4(b)] of color image "Pepper" (threshold $T = 15$). (b) Output of 5×5 MCQR edge detector of order $i = 5$ applied on the hue component [Fig. 5(a)] of test image "Pepper" corrupted by 10% impulsive noise of impulse value 255 acting independently on each RGB channel (threshold $T = 18$).

The output of the proposed edge detectors applied on the hue component of color images can be seen in Fig. 11. Both edge images are thresholded by the threshold that gave the best visual results. It can be seen that the performance of the proposed edge detectors in the presence of noise is very good. It is worthwhile to note here that hue edges do not necessarily coincide with edges found by applying color edge detectors in the RGB domain. For example, edges caused by highlights or shadows will be more prominent in RGB edge maps than in hue edge maps.

V. Conclusion

In this paper, we have proposed a number of digital filters (circular mean, circular median, circular α-trimmed mean filter, and circular modified trimmed mean filter) for angular signals. Some significant properties have been derived for the circular median filter. The application of those filters in the filtering of noisy 1-D angular signals and hue images gave good results for a variety of noise types. Measures of angular dispersion have also been used to propose edge operators for

angular data. Three ways to extend the notion of quasirange to circular data were introduced, and the theoretical output pdf for two of them was derived. Those circular quasiranges were used successfully as edge detectors on hue images. Their comparative performance in noisy edges has been evaluated using quantitative criteria.

APPENDIX A

Suppose that $X_1, X_2, \ldots X_N$ are N i.i.d angular random variables that are distributed according to $f(x)$ distribution function, and denote X_{ADM} as the arc distance median of those variables. The event $B = \{x < X_{\mathrm{ADM}} < x + dx\}$ can occur if one of the random variables, e.g., X_i, lies in the interval $(x, x+dx)$, and the values of the rest $N-1$ variables are such that X_i minimizes d_0 in (5). Therefore, the probability of B, which equals $f_{\mathrm{ADM}}(x)\,dx$, is given by

$$\mathrm{Prob}(B) = f_{\mathrm{ADM}}(x)\,dx = Nf(x)\,dx \int_0^{2\pi}\int_0^{2\pi}\cdots\int_0^{2\pi} f(w_1)\cdots f(w_{N-1})\mathbf{I}(A)\,dw_1\cdots dw_{N-1} \quad \text{(A.1)}$$

and consequently

$$f_{\mathrm{ADM}}(x) = Nf(x) \int_0^{2\pi}\int_0^{2\pi}\cdots\int_0^{2\pi} f(w_1) \cdots f(w_{N-1})\mathbf{I}(A)\,dw_1\cdots dw_{N-1}. \quad \text{(A.2)}$$

Multiplicative constant N appears in the previous expression because each of the N variables is equally likely to be the ADM.

APPENDIX B

It can be easily proven that (11) satisfies

$$\int_0^{2\pi} f(\theta)\,d\theta = 1. \quad \text{(B.1)}$$

Therefore, $f(\theta)$ is appropriate for pdf of an angular variable. The maximum likelihood estimator T_n of location for a given distribution minimizes

$$-\sum_{i=1}^{n} \ln f(\theta_i - T_n). \quad \text{(B.2)}$$

By substituting $f(\theta)$ in the previous expression, we have

$$-\sum_{i=1}^{n}\left[\ln\left(\frac{1}{2(1-e^{-\pi})}\right) + |\pi - |\theta_i - T_n|| - \pi\right] = n\ln(2(1-e^{-\pi})) + n\left(\pi - \frac{1}{n}\sum_{i=1}^{n}|\pi - |\theta_i - T_n||\right). \quad \text{(B.3)}$$

In Section II-A, we have seen that ADM minimizes

$$d_0 = \pi - \frac{1}{n}\sum_{i=1}^{n}|\pi - |\theta_i - a||. \quad \text{(B.4)}$$

Since the other term of the sum is constant, ADM minimizes (B.2), and therefore, it is the MLE of location for this distribution.

APPENDIX C

We will derive the output pdf of CQR applied on a noisy edge of the form (25), assuming that $0 \le m_{s1} < m_{s2} < m_n < 2\pi$ and that when all three kinds of points m_{s1}, m_{s2}, m_n are present, the circular range w equals $m_n - m_{s1}$, i.e.,

$$m_n - m_{s1} = \min\{m_n - m_{s1}, 2\pi - (m_{s2} - m_{s1}) \; 2\pi - (m_n - m_{s2})\}. \quad \text{(C.1)}$$

Analogous expressions can be found for all the other cases. We will first derive the output for the case where the window of the edge operator is on the constant signal region on the left of the edge. Let S, I be the number of signal and impulse points, respectively, that exist inside the window. It is obvious that $S + I = N$. The probability of having exactly I impulses inside the window is

$$P_I = \binom{N}{I} p^I (1-p)^{N-I}. \quad \text{(C.2)}$$

The output y of the detector can take only two values i.e., $y = 0$ and $y = \mathrm{arc}(m_{s1}, m_n)$. The probability of the event $y = 0$ equals

$$\sum_{k=0}^{i}\binom{N}{k}p^k(1-p)^{N-k} + \sum_{k=N-i}^{N}\binom{N}{k}p^k(1-p)^{N-k} \quad \text{(C.3)}$$

whereas probability of the event $y = \mathrm{arc}(m_{s1}, m_n)$ is

$$\sum_{k=i+1}^{N-i-1}\binom{N}{k}p^k(1-p)^{N-k}. \quad \text{(C.4)}$$

The same analysis holds for the case where the edge operator window is over the constant signal area on the right side of the edge. The only difference is that now, the output can be either 0 or $\mathrm{arc}(m_{s2}, m_n)$.

The analysis is more complex when the window is on the actual edge. Let N_1, N_2 be the number of points in the window that belong to the homogeneous regions left and right of the step edge, respectively. In addition, let I_1, S_1 be the number of impulses and signal points that exist in the part of the window that lies to the left side of the edge, and let I_2, S_2 be the number of impulses and signal points in the part of the window that lies to the right side of the edge. In this case

$$N_1 + N_2 = N, \quad I_1 + S_1 = N_1, \quad I_2 + S_2 = N_2 \quad \text{(C.5)}$$

will hold. For a fixed value of N_1, N_2, i.e., for a certain position of the edge detector window over the edge, the probability of the event $\{I_1$ *impulses exist in the part of the window on the left side of the edge and* I_2 *impulses in the part of the window on the right side of the edge*$\}$ is given by the expression

$$P_{I1,I2} = \binom{N_1}{I_1}\binom{N_2}{I_2}p^{(I_1+I_2)}(1-p)^{(N-I_1-I_2)}. \quad \text{(C.6)}$$

For some values of I_1, I_2, the points inside the window can have only two different values. These cases are the following.

- $I_1 = I_2 = 0$. The probability of this event is $(1-p)^N$. In this case, inside the operator window exist N_1 points

of value m_{s1} and N_2 points of value m_{s2}, and the output of the edge detector can be either 0 or arc(m_{s1}, m_{s2}).

- $I_1 = N_1$, $I_2 = N_2$. In this case, all points inside the operator window are impulses of value m_n, and therefore, the output of the detector is zero. The probability of this event is p^N.
- $I_1 = N_1$, $I_2 \neq N_2$. The probability of this event depends on I_2 and is given by

$$p^{N_1}\binom{N_2}{I_2}p^{I_2}(1-p)^{N_2-I_2}. \tag{C.7}$$

In this case, the points inside the window whose value is m_n are $N_1 + I_2$, and the points having value m_{s2} are $N_2 - I_2$. The output of the detector is in (C.8), shown at the bottom of the page. The probability of y being either 0 or arc(m_n, m_{s2}) is given by the sum of (C.7) for all I_2 satisfying the corresponding inequalities in (C.8).

- $I_2 = N_2$, $I_1 \neq N_1$. This case can be handled exactly like the previous one.

For all the other value combinations of I_1, I_2, the points inside the window can have one of three different values, i.e., m_{s1}, m_{s2}, m_n, and the output of the edge operator can take one of four values as in

$$V_1 = m_n - m_{s1}, \quad V_2 = m_n - m_{s2}$$
$$V_3 = 0, \quad V_4 = m_{s2} - m_{s1}.$$

In this case, (C.9), shown at the bottom of the page, holds for the detector output, where A_i are the corresponding events. As a consequence, the probability of the event $y = V_i$ is given by

$$P_{V_i} = \sum_{I_1=0}^{N_1-1}\sum_{I_2=0}^{N_2-1} P_{I_1,I_2}\mathbf{I}(A_i), \quad \text{for } (I_1, I_2) \neq (0,0) \tag{C.10}$$

where $\mathbf{I}(A_i)$ is the indicator function that equals unity when the event A_i holds and zero otherwise.

Appendix D

Suppose that we have N i.i.d. angular variables $X_1, \ldots, X_N$. The joint pdf of the Cartesian ordered random variables $X_{(1)}, \ldots, X_{(N)}$ is given by [18]

$$f_{X_{(1)},\ldots,X_{(N)}}(x_1,\ldots,x_N) = N! \cdot f(x_1)f(x_2)\cdots f(x_N)u(x_2-x_1)\cdots u(x_N-x_{N-1}) \tag{D.1}$$

where $u(x)$ is the unit step function. The joint pdf of all N random variables T_k in (26) for order $i = 0$, i.e., $\Delta = 1$, cannot be evaluated directly since T_k are linearly dependent, and their Jacobian is zero. Instead, we evaluate the joint pdf of the $N-1$ random variables $T_k, k = 1, \ldots, N-1$ by using an auxiliary r.v. $v = X_{(N)}$. Using the formula for the joint pdf of functions of random variables [19], we can prove that the joint pdf of $v, T_1, \ldots, T_{N-1}$ will have the form

$$f_{v,T_1,\ldots,T_{N-1}} = N! \cdot u(T_1)\cdots u(T_{N-1}) \cdot f(v - T_{N-1} - \cdots - T_1) \times f(v - T_{N-1} - \cdots - T_2)\cdots f(v - T_{N-1})f(v). \tag{D.2}$$

The joint pdf of T_k, $k = 1, \ldots, N-1$ can be easily derived by integrating (D.2) with respect to v as

$$f_{T_1,\ldots,T_{N-1}} = N! \cdot u(T_1)\cdots u(T_{N-1}) \cdot \int_0^{2\pi} f(v - T_{N-1} - \cdots - T_1)\cdots f(v - T_{N-1})f(v)\,dv. \tag{D.3}$$

Using the previous result and the fact that $\sum_{k=1}^{N} T_k = 2\pi$, we can write the joint pdf of all T_i in the form

$$f_{T_1,\ldots,T_N} = N! \cdot u(T_1)\cdots u(T_{N-1}) \cdot \delta(2\pi - T_1 - \cdots - T_N) \cdot \int_0^{2\pi} f(v - T_{N-1} - \cdots - T_1)f(v - T_{N-1} - \cdots - T_2)\cdots f(v - T_{N-1})f(v)\,dv \tag{D.4}$$

where $\delta(x)$ is the delta function. Now, we can proceed in finding the pdf of the maximum T_k. Since T_k are dependent random variables, we cannot use the well-known formula for the pdf of order statistics of iid random variables [18]. Instead, the probability the T_k to be maximum and equal to x will be evaluated for each k separately. The probability a certain T_k to be maximum among $T_1, \ldots, T_N$ and equal to x equals the probability of T_k to be x and all the other T_i to be smaller than x

$$\begin{aligned}&\text{Prob}(T_k = x \text{ and } T_k = \max(T_1,\ldots T_N))\\ &= \text{Prob}(T_k = x \text{ and } T_1 < x \text{ and}\\ &\quad \cdots T_{k-1} < x \text{ and } T_{k+1} < x \cdots \text{ and } T_N < x)\\ &= dx \cdot \int_0^x \cdots \int_0^x f_{T_1,\ldots,T_N}(v_1,\ldots,v_{i-1},x\\ &\quad v_{i+1},\ldots,v_N)\,dv_1\cdots dv_{i-1}\,dv_{i+1}\cdots dv_N.\end{aligned} \tag{D.5}$$

$$y = \begin{cases} 0 & 0 < N_1 + I_2 \leq i \quad \text{or} \quad N - i \leq N_1 + I_2 \leq N \\ \text{arc}(m_n, m_{s2}) & i+1 \leq N_1 + I_2 \leq N - i - 1 \end{cases} \tag{C.8}$$

$$y = \begin{cases} V_1 & i < I_1 + I_2 \quad \text{and} \quad i < N_1 - I_1, & (A_1)\\ V_2 & i < I_1 + I_2 \quad \text{and} \quad N_1 - I_1 \leq i < N - I_1 - I_2, & (A_2)\\ V_3 & (i < I_1 + I_2 \quad \text{and} \quad N - I_1 - I_2 \leq i) \text{ or} & \\ & (I_1 + I_2 \leq i < N_2 + I_1 \quad \text{and} \quad N_1 - I_1 \leq i < N - I_1 - I_2) \text{ or} & \\ & (N_2 + I_1 \leq i < N), & (A_3)\\ V_4 & I_1 + I_2 \leq i < N_2 + I_1 \quad \text{and} \quad i < N_1 - I_1, & (A_4) \end{cases} \tag{C.9}$$

The sum of these probabilities for all T_k, $k = 1, \ldots, N$ will be equal to $f_{T_{\max}}(x)\,dx$. Therefore, $f_{T_{\max}}$ is given by

$$f_{T_{\max}}(x) = \int_0^x \cdots \int_0^x f_{T_1,\ldots,T_N}(x, v_2, \ldots, v_N)\,dv_2 \cdots dv_N + \int_0^x \cdots \int_0^x f_{T_1,\ldots,T_N}(v_1, x, \ldots, v_N)\,dv_1\,dv_3 \cdots dv_N + \cdots + \int_0^x \cdots \int_0^x f_{T_1,\ldots,T_N}(v_1, v_2, \ldots, x)dv_1 \cdots dv_{N-1}. \quad \text{(D.6)}$$

Since MCQR W_0 is given by (21), its output pdf will be

$$f_{W_0}(x) = f_{T_{\max}}(2\pi - x). \quad \text{(D.7)}$$

By substituting (D.4) in (D.7) and using (D.7) and properties of the delta function, we obtain (29).

REFERENCES

[1] J. Foley, A. van Dam, S. Feiner, and J. Hughes, *Computer Graphics: Principles and Practice*. Reading, MA: Addison-Wesley, 1990.

[2] B. C. Lovell and R. C. Williamson, "The statistical performance of some instantaneous frequency estimators," *IEEE Trans. Signal Processing*, vol. 40, pp. 1708–1723, July 1992.

[3] P. E. Trahanias and A. N. Venetsanopoulos, "Vector directional filters—A new class of multichannel image processing filters," *IEEE Trans. Image Processing*, vol. 2, pp. 528–534, Oct. 1993.

[4] K. N. Plataniotis, D. Androutsos, and A. N. Venetsanopoulos, "Color image processing using fuzzy vector directional filters," in *Proc. IEEE Workshop Nonlinear Signal Image Process.*, June 1995, pp. 535–538.

[5] K. V. Mardia, *Statistics of Directional Data*. New York: Academic, 1972.

[6] P. E. Jupp and K. V. Mardia, "A unified view of the theory of directional statistics, 1975–1988," *Int. Stat. Rev.*, vol. 57 no. 3, pp. 261–294, 1989.

[7] F. Perez and C. Koch, "Hue color segmentation determines object boundaries," *Int. J. Comput. Vision*, vol. 12, pp. 17–42, 1994.

[8] K. Sobottka and I. Pitas, "Face localization and facial feature extraction based on shape and color information," in *Proc. IEEE Int. Conf. Image Process.*, Sept. 1996, vol. III, pp. 483–486.

[9] P. E. Trahanias, D. Karakos, and A. N. Venetsanopoulos "Directional segmentation of color images," in *Proc. IEEE Workshop Nonlinear Signal Image Process.*, June 1995, pp. 515–518.

[10] P. H. Gregson, "Using angular dispersion of gradient direction for detecting edge ribbons," *IEEE Trans. Pattern Anal. Machine Intell.*, vol. 15, pp. 682–696, July 1992.

[11] I. Pitas and A. N. Venetsanopoulos, *Nonlinear Digital Filters: Principles and Applications*. Boston, MA: Kluwer, 1990.

[12] R. Liu and K. Singh, "Ordering directional data: Concepts of data depth on circles and spheres," *Ann. Stat.*, vol. 20, no. 3, pp. 1468–1484, 1992.

[13] B. J. Justusson, "Median filtering: Statistical properties," in *Topics in Applied Physics*, vol. 43, T. S. Huang, Ed. New York: Springer-Verlag, 1981.

[14] N. Nikolaidis and I. Pitas, "Directional statistics in nonlinear vector field filtering," *Signal Process.*, vol. 38, pp. 299–316, 1994.

[15] D. Collet, "Outliers in circular data," *Appl. Stat.*, vol. 29, no. 1, pp. 50–57, 1980.

[16] N. Nikolaidis and I. Pitas, "Optimal L-filters for vector magnitude filtering," in *Proc. Euro. Signal Process. Conf. (EUSIPCO)*, 1994, pp. 955–959.

[17] A. K. Jain, *Fundamentals of Digital Image Processing*. Englewood Cliffs, NJ: Prentice-Hall, 1989.

[18] H. A. David, *Order Statistics*. New York: Wiley, 1980.

[19] A. Papoulis, *Probability, Random Variables and Stochastic Processes*. New York: McGraw-Hill, 1984.

Nikos Nikolaidis (S'93–M'98) was born in Kozani, Greece, in 1968. He received the diploma of electrical engineering (with highest honors) in 1991 and the Ph.D. degree in electrical engineering in 1997, both from the University of Thessaloniki, Thessaloniki, Greece.

From 1992 to 1996, he served as Teaching Assistant in the Departments of Electrical Engineering and Informatics at the University of Thessaloniki. He is currently with the Artificial Intelligence and Information Analysis Laboratory, University of Thessaloniki. His research interests include multichannel signal processing, nonlinear image processing and analysis, copyright protection of digital images, and 3-D image processing.

Dr. Nikolaidis is a member of the Technical Chamber of Greece.

Ioannis Pitas (SM'97) received the diploma of electrical engineering in 1980 and the Ph.D. degree in electrical engineering in 1985, both from the University of Thessaloniki, Thessaloniki, Greece.

Since 1994, he has been Professor with the Department of Informatics, University of Thessaloniki. From 1980 to 1993, he served as Scientific Assistant, Lecturer, Assistant Professor, and Associate Professor with the Department of Electrical and Computer Engineering, University of Thessaloniki. He served as a Visiting Research Associate with the University of Toronto, Toronto, Ont., Canada, the University of Erlangen-Nuernberg, Erlangen, Germany, Tampere University of Technology, Tampere, Finland, and as Visiting Assistant Professor at the University of Toronto. He was lecturer in short courses for continuing education. His current interests are in the areas digital image processing, multidimensional signal processing, and computer vision. He has published over 250 papers and contributed to eight books in his area of interest. He is the co-author of the book *Nonlinear Digital Filters; Principles and Applications* (Boston, MA: Kluwer, 1990). He is author of the book *Digital Image Processing Algorithms* (Englewood Cliffs, NJ: Prentice-Hall, 1993). He is editor of the book *Parallel Algorithms and Architectures for Digital Image Processing, Computer Vision and Neural Networks* (New York: Wiley, 1993).

Dr. Pitas has been member of the European Community ESPRIT Parallel Action Committee. He has also been invited speaker and/or member of the program committee of several scientific conferences and workshops. He is Associate Editor of the IEEE TRANSACTIONS ON CIRCUITS AND SYSTEMS and co-editor of *Multidimensional Systems and Signal Processing*. He was chair of the 1995 IEEE Workshop on Nonlinear Signal and Image Processing (NSIP95).